Improved two-dimensional cracked finite element for crack fault diagnosis

Aysha Kalanad, B.N. Rao

Structural Engineering Division, Department of Civil Engineering
Indian Institute of Technology Madras
Chennai 600 036, India
e-mail: bnrao@iitm.ac.in

In this paper the two-dimensional finite element with an embedded edge crack proposed by Potirniche et al. (2008) is improved further for crack depth ratios ranging up to 0.9 and for predicting the natural frequency of a cracked beam more accurately. The element is implemented in the commercial finite element code ABAQUS as user element subroutine. The accuracy of the proposed improved cracked element is verified by comparing the predicted, first natural frequency with available experimental data. Subsequently, a methodology to detect the crack's location and size in conjunction with the proposed improved cracked element is also presented.

Keywords: cracked finite element, user element, ABAQUS, natural frequency, crack fault diagnosis.

NOMENCLATURE

c	–	Distance of crack from end of beam
E	–	Modulus of elasticity
F_i	–	Nodal force
F_f	–	Geometric factor for single edge notch strip under tension loading
F_m	–	Geometric factor for single edge notch strip under bending loading
F_I	–	Mode I geometric factor for vertical nodal force
F_{II}	–	Mode II geometric factor for vertical nodal force
h	–	Height of element
H	–	Height of beam
K_I, K_{II}	–	Stress Intensity Factor for mode I and mode II
K_{ij}	–	Components of stiffness matrix
L	–	Length of beam
t	–	Thickness
u_i	–	Nodal displacement
w	–	Width of element
α	–	Crack depth
ν	–	Poisson's ratio
ρ	–	Density
ω	–	Natural frequency of uncracked beam
ω_c	–	Natural frequency of cracked beam

1. INTRODUCTION

The quantitative diagnosis of structural cracks through nondestructive testing is an important part of predicting structural integrity and reliability of components for a wide range of civil, mechanical and aeronautical engineering applications. Due to the practical importance of an early detection of cracks, the crack identification problem in structures has been extensively investigated and has led to the development of various methods. The presence of a crack drastically affects the dynamic behavior of structures. Depending on the location and size of the crack, the stiffness of the structure is reduced and, therefore, so are its natural frequencies compared to the original crack free structure. Many researchers have used the above characteristics to detect and locate cracks and a plethora of vibration-based methods for crack detection has been developed [2, 14, 16, 20–22, 25, 28].

The most useful damage localization methods based on vibration measurements are probably those based on changes in natural frequencies and mode shapes. Reviews of research works dealing with the problem of crack detection based on changes in modal parameters can be found in the published literature [8, 19, 27, 32]. Shift in natural frequencies has been commonly used to investigate the location and size of crack. For example, some research works [9, 15, 22] have been devoted to the identification of the location and size of crack through the determination of the intersection point of the superimposed contours corresponding to the measured eigenfrequency variations due to the crack. This damage identification technique is called the "frequency contour lines method". In order to avoid the problem of a non-unique damage location in the case of a structural symmetric beam, Swamidas et al. [33] proposed to extend this crack identification method by adding an off-center mass to the simply-supported beam. Sinou [30, 31] developed an extension of the frequency contour lines method based on the changes of frequency ratios in the cracked beam, thus avoiding the need for accurate knowledge of the material properties and frequencies of the crack- free beam. Moreover, Owolabi et al. [23] proposed a crack identification technique based not only on the measured changes in the first three natural frequencies (i.e., the frequency contour lines method), but also in the corresponding amplitudes of the measured acceleration frequency response functions. Using the frequency contours and amplitude contours of the first three modes, they demonstrated that the location and size of crack can be determined uniquely. Dilena and Morassi [5, 6] proved that the measurement of an appropriate set of frequencies and antiresonance frequencies enables unique identification of damage. The theoretical results were confirmed by comparisons with numerical and experimental tests. Dilena and Morassi [7] also suggested that the direction in which the nodal points move can point to the damage location.

Several approaches have been used to model the problem of a cracked beam using the finite element method. One-dimensional cracked beam finite elements for vibration studies have been developed previously by other researchers [3, 4, 11, 13, 17, 24]. With the aim to simulate the crack presence without actually modeling the crack, more recently a two-dimensional cracked finite element was developed by Potirniche et al. [26] for fatigue and fracture applications. In this approach, the influence of the additional flexibility of the element due to the crack presence was derived from the Castigliano's first theorem using fracture mechanics concepts. However, the accuracy of the predicted natural frequency using the cracked finite element developed by Potirniche et al. [26] for higher values of crack depth ratios is less. Assuming that the applied shear forces results only in mode II stress intensity factors (SIF), Potirniche et al. [26] derived the components of the stiffness matrix for the cracked element, adopting the geometrical factor (for the effect of boundary conditions at free edge) corresponding to pure shear for infinite boundary conditions given in Tada et al. [34]. It should be noted that the pure shear condition can only be reproduced when the shear force acting along the edge of the cracked element, is accompanied by shear forces acting on the other three edges. However, when the applied shear force acts along the edge of the cracked element without accompanying shear forces on the other three edges, as considered in Potirniche et al. [26], mixed-mode conditions prevail instead of the pure shear condition, which results in both mode I and mode II SIFs. In addition, the adopted geometrical factor should take into account both the effect of finite size of the cracked element and the effect of boundary conditions at the free edge.

Hence, this study is aimed at further improvement of the two-dimensional finite element with an embedded edge crack proposed by Potirniche et al. [26].

This paper presents an improved two-dimensional finite element with an embedded edge crack for crack depth ratios ranging up to 0.9 and for predicting the natural frequency of a cracked beam more accurately. The element is implemented in the commercial finite element code ABAQUS as user element (UEL) subroutine. The accuracy of the UEL is verified by comparing the frequency response of various beams with the edge crack under bending. Later, a methodology to detect the crack location and size in conjunction with the proposed improved cracked element is presented for singularity problems like a cracked beam.

2. IMPROVED CRACKED FINITE ELEMENT

For predicting the natural frequency of a cracked beam more accurately, in this section, the following improvements to the cracked finite element originally developed by Potirniche et al. [26] are presented: (a) to handle crack depth ratios ranging up to 0.9; and (b) the additional flexibility of the cracked element due to the applied shear forces. Consider the cracked finite element with the node numbering and the degrees of freedom per node as shown in Fig. 1a the mathematical definition details of which are given in Potirniche et al. [26].

In Fig. 1b, the tensile force at node 3 gives a force and a moment, both of which contribute to the opening of the crack. Hence, the contribution K_{IF_3} of the nodal force F_3 at node 3 is summation of the SIFs given by the force and the resulting bending moment $F_3 h/2$ (h is the element depth), which can be written as

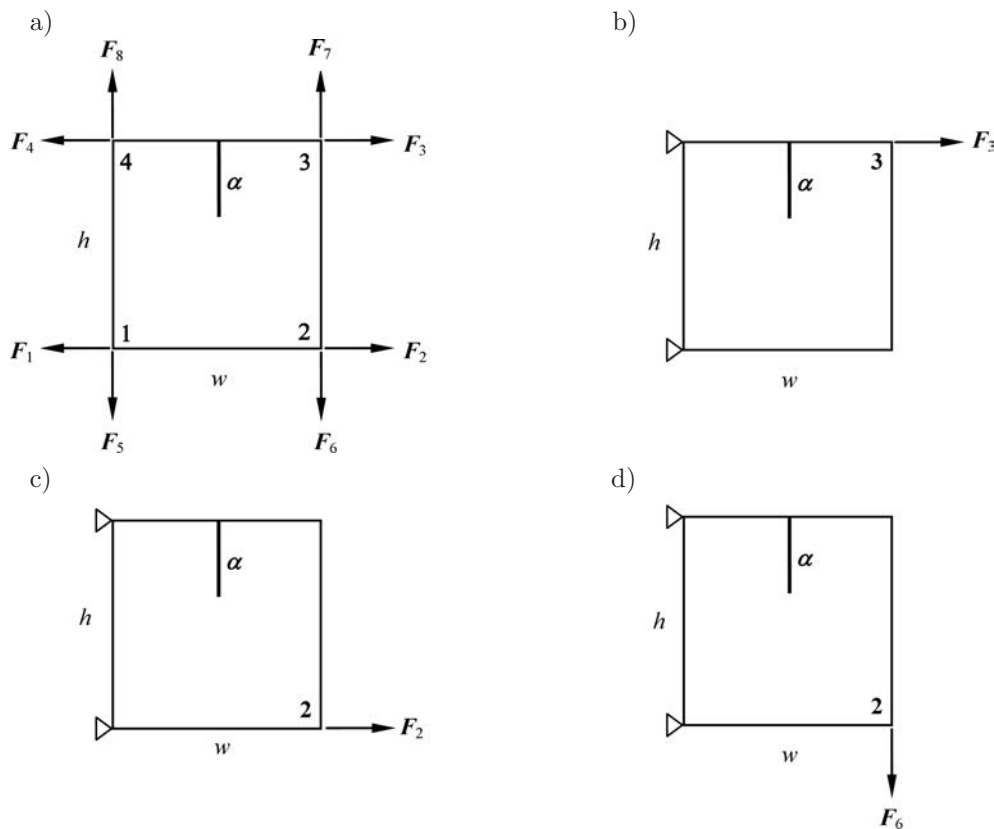$$K_{IF_3} = K_{IF_3}^{f} + K_{IF_3}^{m}, \tag{1}$$

Fig. 1. Two-dimensional cracked finite element: a) node numbering and degrees of freedom at all nodes, b) nodal force F_3 at node 3, c) nodal force F_2 at node 2, and d) nodal force F_6 at node 2.

where

$$K_{IF_3}^f = F_f \frac{F_3}{ht}\sqrt{\pi\alpha} \qquad \text{and} \qquad K_{IF_3}^m = F_m \frac{3F_3}{ht}\sqrt{\pi\alpha}, \tag{2}$$

with t being the element thickness.

The FRANC2DL finite element code [10, 12, 35, 36] is used with the $J-$integral option to extract the SIFs from stress strain fields around the crack tip location. Two-dimensional, finite element models having $w/h = 2$ with degrees of freedom ranging from 3510 (for the case $\alpha/h = 0.1$) to 4258 (for the case $\alpha/h = 0.9$), along with a ring of six-noded quarter-point elements around the crack tip and eight-noded elements elsewhere are used under plane stress conditions. The minimum element size at the crack tip location is $0.0025w$. Crack length to depth ratios (α/h) are varied from 0.1 to 0.9 with nodal forces applied at various locations on the cracked element. Using the SIFs values obtained from FRANC2DL for α/h ranging from 0.1 to 0.9, and Eq. (2), the geometrical factors F_f and F_m, for the cracked element under tensile and bending loading respectively, are obtained by curve fitting techniques as a function of α/h, as follows:

$$F_f\left(\frac{\alpha}{h}\right) = 2.6233 - 51.173\frac{\alpha}{h} + 551.45\left(\frac{\alpha}{h}\right)^2 - 2563.7\left(\frac{\alpha}{h}\right)^3 + 5883.6\left(\frac{\alpha}{h}\right)^4$$
$$- 6472.2\left(\frac{\alpha}{h}\right)^5 + 2750.4\left(\frac{\alpha}{h}\right)^6 \tag{3}$$

and

$$F_m\left(\frac{\alpha}{h}\right) = 1.6426 - 18.687\frac{\alpha}{h} + 192.08\left(\frac{\alpha}{h}\right)^2 - 883.57\left(\frac{\alpha}{h}\right)^3 + 2018.3\left(\frac{\alpha}{h}\right)^4$$
$$- 2213.7\left(\frac{\alpha}{h}\right)^5 + 939\left(\frac{\alpha}{h}\right)^6. \tag{4}$$

The above given geometrical factors F_f and F_m are validated for other cases with $w/h > 2.0$ by comparing the SIFs values obtained from FRANC2DL with those values obtained using Eq. (2) in conjunction with Eq. (3) and (4). The effect of w/h is found to be practically negligible for $w/h \geq 2.0$.

Contrary to the tensile force acting at node 3 (in Fig. 1b), as discussed above, in Fig. 1c the nodal force F_2 acting at node 2 results in a force that leads to the opening of the crack and a resolved bending moment that leads to the closing of the crack. Hence, the contribution K_{IF_2} of the nodal force F_2 at node 2 can be written as

$$K_{IF_2} = K_{IF_2}^f - K_{IF_2}^m, \tag{5}$$

where

$$K_{IF_2}^f = F_f \frac{F_2}{ht}\sqrt{\pi\alpha} \qquad \text{and} \qquad K_{IF_2}^m = F_m \frac{3F_2}{ht}\sqrt{\pi\alpha}, \tag{6}$$

with the geometrical factors F_f and F_m defined in Eq. (3) and (4).

Following the procedure based on Castigliano's first theorem, outlined in Potirniche et al. [26] the stiffness components K_{2j} and K_{3j} can be obtained using the geometrical factors F_f and F_m defined in Eq. (3) and (4). The stiffness components K_{1j} and K_{4j} can also be obtained following the same procedure as that for the stiffness components K_{2j} and K_{3j}.

In Fig. 1d the nodal force F_6 acting at node 2 gives a shear force and a moment (Fw), both of which contribute to mode I and II SIFs, which can be written as

$$K_{IF_6} = F_I \frac{6Fw}{h^2t}\sqrt{\pi\alpha} \quad \text{and} \quad K_{IIF_6} = F_{II}\frac{F}{ht}\sqrt{\pi\alpha} . \tag{7}$$

Using the SIFs values obtained from FRANC2DL for α/h ranging from 0.1 to 0.9, and Eq. (7), the geometrical factors for the cracked element F_I and F_{II}, respectively, are obtained by curve fitting techniques as a function of α/h as follows:

$$F_I\left(\frac{\alpha}{h}\right) = 0.821 - 9.344\frac{\alpha}{h} + 96.04\left(\frac{\alpha}{h}\right)^2 - 441.78\left(\frac{\alpha}{h}\right)^3 + 1009.15\left(\frac{\alpha}{h}\right)^4$$
$$- 1106.85\left(\frac{\alpha}{h}\right)^5 + 469.5\left(\frac{\alpha}{h}\right)^6, \quad (8)$$

and

$$F_{II}\left(\frac{\alpha}{h}\right) = 1.018 - 17.794\frac{\alpha}{h} + 162.7\left(\frac{\alpha}{h}\right)^2 + 596.45\left(\frac{\alpha}{h}\right)^3 + 1098.3\left(\frac{\alpha}{h}\right)^4$$
$$- 994.94\left(\frac{\alpha}{h}\right)^5 + 353.26\left(\frac{\alpha}{h}\right)^6. \quad (9)$$

The stiffness components K_{6j} can be obtained adopting the following procedure. Using Castigliano's first theorem, the difference between the nodal forces in the cracked (F_i) and uncracked (F_i^0) cases can be obtained by taking the partial derivatives of the SIFs with respect to the corresponding displacements (u_i) by the relation [34],

$$F_6^0 - F_6 = \frac{2t}{E'}\left[\int_0^\alpha K_I\frac{\partial K_I}{\partial u_6}da + \int_0^\alpha K_{II}\frac{\partial K_{II}}{\partial u_6}da\right], \quad (10)$$

where $E' = E$ for plane stress, $E' = E/(1 - \nu^2)$ for plane strain, E and ν are the modulus of elasticity and Poisson's ratio, respectively. Replacing the SIFs in the above equation with their respective formulas in Eq. (7) and after some simplifications, one obtains:

$$F_6^0 - F_6 = \frac{2\pi}{E'h^2t}\left[\frac{36w^2}{h^2}\int_0^\alpha aF_I^2da + \int_0^\alpha aF_{II}^2da\right]F_6\frac{\partial F_6}{\partial u_6}. \quad (11)$$

Defining A_{66} as

$$A_{66} = \frac{2\pi}{E'h^2t}\left[\frac{36w^2}{h^2}\int_0^\alpha aF_I^2da + \int_0^\alpha aF_{II}^2da\right], \quad (12)$$

and noting that

$$\frac{\partial F_6}{\partial u_6} = K_{66}, \quad (13)$$

the relation between the two nodal forces for the uncracked and cracked elements becomes

$$F_6^0 = (1 + A_{66}K_{66})F_6. \quad (14)$$

Using $\{F^0\} = [K^0]\{u\}$, Eq. (14) can be written as

$$\sum_{j=1}^8 K_{6j}^0 u_j = \sum_{j=1}^8 (1 + A_{66}K_{66})K_{6j}u_j, \quad (15)$$

which is valid only if the coefficients multiplying the independent variables u_j on both sides of the above equation are equal,

$$K_{6j}^0 = (1 + A_{66}K_{66})K_{6j} \qquad \text{for} \qquad j = 1, 2, \ldots, 8. \quad (16)$$

Solving Eq. (16) for K_{6j} the solution is found to be

$$K_{66} = \frac{-1 + \sqrt{1 + 4A_{66}K_{66}^0}}{2A_{66}}, \quad (17)$$

and

$$K_{6j} = \frac{2K_{6j}^0}{1 + \sqrt{1 + 4A_{66}K_{66}^0}} \qquad \text{for} \qquad j = 1, 2, \ldots, 8 \qquad \text{and} \qquad j \neq 6. \quad (18)$$

Similar formulas can be obtained for all the components K_{5j}, K_{7j} and K_{8j}.

3. VALIDATION OF CRACKED FINITE ELEMENT

The proposed improved two-dimensional finite element with an embedded edge crack is implemented in the commercial finite element code ABAQUS [1] as a User Element Fortran subroutine (UEL.f). The performance of the proposed improved finite element is demonstrated by comparing the frequency ratio (ω_c/ω) (ratio of the natural frequency of the cracked beam to that of the uncracked beam) versus the crack depth ratio (α/H) (the ratio of the crack depth (α) to the beam height (H)) results obtained using UEL, with the reported results in the literature, for the bending mode, for various crack location ratios (c/L) (ratio of the crack location to the beam length). The following beam cases are considered: (1) Simply supported beam with a double edge surface crack at mid-span; (2) Cantilever beam with a surface crack at 20% of the beam span from fixed end; and (3) Simply supported beam with a surface crack at mid-span. In the numerical study the crack depth ratio (α/H) is varied from 0 to 0.5.

3.1. Simply supported beam with a double edge surface crack

In this numerical example, a steel beam [3] having the length $L = 0.575$ m, the height $H = 0.03175$ m, the thickness $t = 0.00952$ m with $E = 2.06 \times 10^{11}$ N/m^2, and $\rho = 7800$ kg/m^3, is considered. Figure 2 shows typical FEM discretization with 36 standard four- node ABAQUS [1] elements and one UEL each at the top and the bottom at the top of the beam for $c/L = 0.5$. Figure 3 shows the first natural frequency ratio (ω_c/ω) versus the crack depth ratio (α/H) for simply supported beam with two surface cracks, at the top and bottom edges of the beam at mid-span. Compared with the predictions obtained using the damaged finite element by Potirniche et al. [26], the first natural frequency reduction predicted by the proposed improved two-dimensional finite element matches very well with the experiments results by Chondros et al. [3].
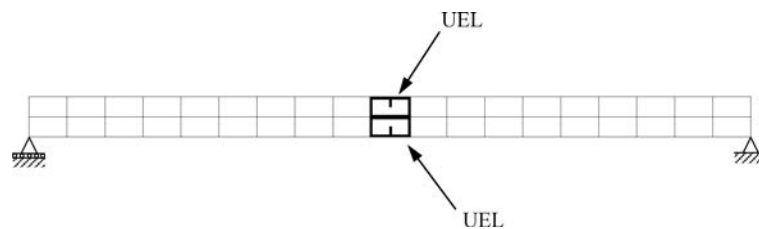

Fig. 2. Discretization of simply supported beam with double edge surface crack using 36 standard four node ABAQUS elements and two UELs.
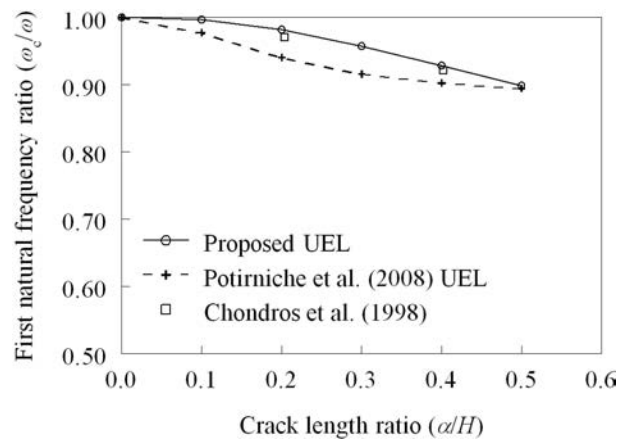

Fig. 3. First natural frequency ratio versus the crack depth ratio for simply supported beam with double edge surface crack at mid-span.

3.2. Cantilever beam with a surface crack

In this numerical example, a steel cantilever beam [37] with all the geometric and material properties same as that of simply supported beam with a double edge surface crack except having the height $H = 0.0242$ m, is considered. Typical FEM discretization with 22 standard four node ABAQUS [1] elements and one UEL for $c/L = 0.2$ measured from fixed end is shown in Fig. 4. Figure 5 shows the first natural frequency ratio (ω_c/ω) versus the crack depth ratio (α/H) for steel cantilever beam with crack located at a distance of 20% of the beam length from the fixed end. Compared with the predictions obtained using the damaged finite element by Potirniche et al. [26], the first natural frequency reduction predicted by the proposed improved two-dimensional finite element matches very well with the experiments results by Wendtland [37]. Contrary to the reported results [26], the current study showed much deviation in the predictions obtained using the damaged finite element by Potirniche et al. [26], when compared with the experiments results by Wendtland [37].
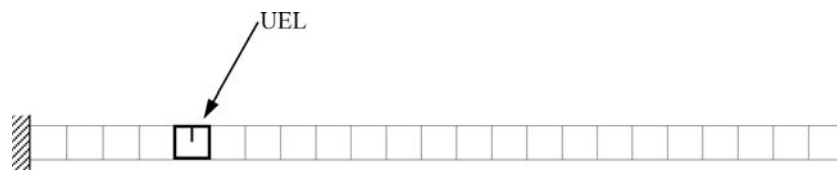

Fig. 4. Discretization of cantilever beam with surface crack using 22 standard four node ABAQUS elements and one UEL.
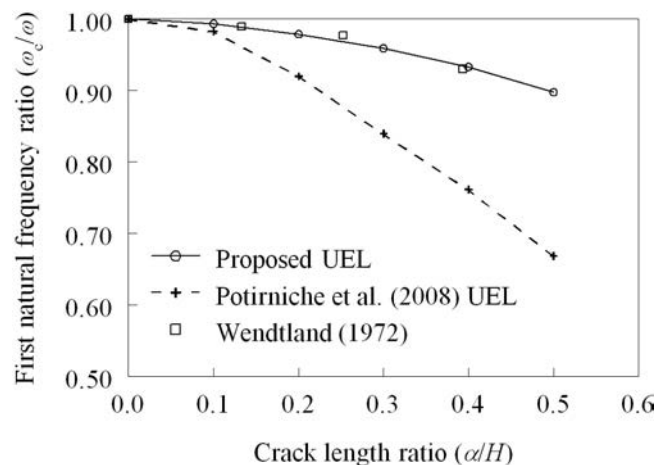

Fig. 5. First natural frequency ratio versus the crack depth ratio for cantilever beam with surface crack at 20% of beam length from fixed end.

3.3. Simply supported beam with a surface crack

An aluminum beam [3] having the length $L = 0.235$ m, the height $H = 0.0254$ m, and the thickness $t = 0.006$ m with the elastic modulus $E = 7.2 \times 10^{10}$ N/m^2 and the density $\rho = 2800$ kg/m^3, is considered. Typical FEM discretization with eight standard four node ABAQUS [1] elements and one UEL for $c/L = 0.5$ is shown in Fig. 6. Figure 7a shows the first natural frequency ratio (ω_c/ω) versus the crack depth ratio (α/H) for simply supported beam with a surface crack at mid-span. Compared with the predictions obtained using the damaged finite element by Potirniche et al. [26], the first natural frequency reduction predicted by the proposed improved two-dimensional finite element matches very well with the experiments results by Chondros et al. [3].

For the simply supported beam case considered above, the FEM discretization with the height of UEL equal to the beam height is adopted. In the following, the effect of the number of elements
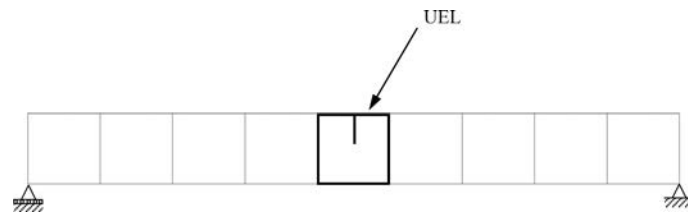
Fig. 6. Discretization of simply supported beam with surface crack using 8 standard four node ABAQUS elements and one UEL.
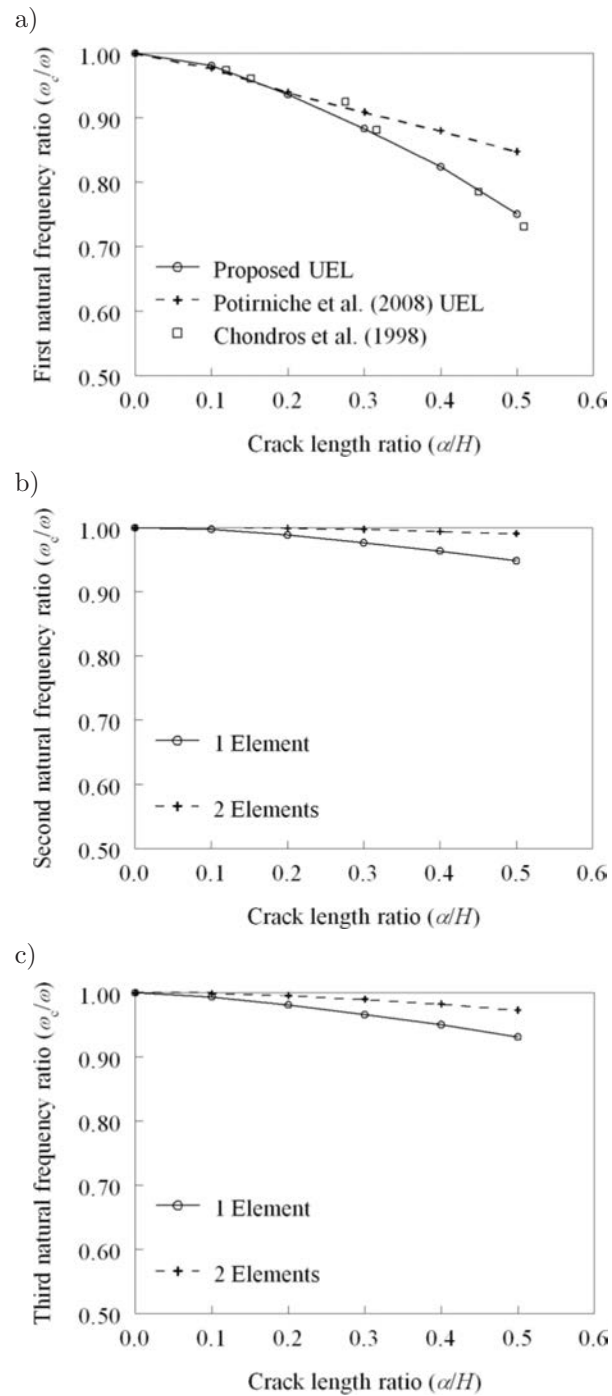

Fig. 7. Variation in natural frequency reduction of simply supported beam with surface crack at mid-span: a) first mode with surface crack at mid-span, b) second mode with surface crack at mid-span, and c) third mode with surface crack at $c/L = 1/3$.

along the direction of the beam height on the accuracy in predicting the reduction in the natural frequencies of higher modes is studied.

Noting that if the crack location coincides with the vibration node of one of the modes, the frequency for that mode remains almost unchanged, Fig. 7b shows variation in the natural frequency reduction of second mode of simply supported beam with a surface crack at mid-span with respect to the number of elements along the direction of the beam height, predicted by the proposed improved two-dimensional finite element for the various values of the crack depth ratios (α/H). Similarly, Fig. 7c shows the variation in the natural frequencies reduction of third mode of simply supported beam with a surface crack at $c/L = 1/3$ measured from the support, with respect to the number of elements along the direction of the beam height. It can be observed from Figs. 7b and 7c that by adopting two elements along the direction of the beam height, better accuracy can be obtained in the prediction of reduction in the natural frequencies of higher modes, which are essential for the predicting the crack location and size. Hence, in the crack identification technique presented in the subsequent sections, two elements along the direction of the beam height are adopted and when the crack depth is equal to the height of UEL, the element stiffness is assumed to be zero.

4. Crack identification procedure

Using the first three natural frequencies obtained using the proposed improved two-dimensional finite element, frequency response functions are approximated using surface fitting techniques available in MATLAB [18]. As the crack location and the crack size influence the changes in the natural frequencies of a cracked beam, a particular frequency can correspond to different crack locations and crack sizes. The frequency contour line resulting from a combination of different crack locations and crack sizes (for a particular mode) can be plotted in a curve with crack location and crack size as its axes [23]. The development of a crack, at a certain location, results in a sudden reduction of the bending stiffness of the beam, and subsequently leads to a shift of the natural frequency. The inverse problem of the crack identification is to predict the crack location ratio (c/L) and crack depth ratio (α/H), once the value of natural frequencies are known. Information of any two natural frequency variations enables one to predict the location and depth of a crack [29]. As the frequency for a mode remains almost unchanged, if the crack location coincides with the vibration node of that mode, a minimum of three curves is required to identify the two unknown parameters of crack location and size.

5. Experimental validation

The crack detection procedure outlined above in conjunction with the proposed improved two-dimensional finite element is validated using: a) the experimental data reported by Silva and Gomes [29], who performed an extensive set of modal analysis experiments on free–free beams with the goal of providing objective data to validate proposed techniques for damage detection and b) the experimental data on fixed-fixed and simply supported beams reported by Owolabi et al. [23].

5.1. Free-free beam

Test specimens adopted by Silva and Gomes [29] were steel beams with 0.032×0.016 m^2 rectangular cross-section and 0.72 m long. The corresponding material properties were: $E = 2.06 \times 10^{11}$ N/m^2; $\nu = 0.29$; and $\rho = 7650$ kg/m^3. In the current study, the same beam is modeled with 73 standard four node ABAQUS [1] elements and one UEL. Typical discretization of free-free beam is shown in Fig. 8. Table 1 presents a satisfactory comparison of the frequency ratio (ω_c/ω) of the first three natural frequencies predicted by the proposed improved two-dimensional finite element with
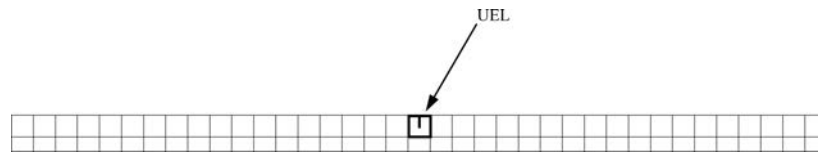
Fig. 8. Discretization of free-free beam with surface crack using 73 standard four node ABAQUS elements and one UEL.

Table 1. Comparison of (ω_c/ω) of first three predicted natural frequencies of free-free beam with experimental data.

Crack case	Actual crack [29]		Mode 1			Mode 2			Mode 3		
	Location c/L	Size α/H	Experiment [29]	Proposed Method	Error [%]	Experiment [29]	Proposed Method	Error [%]	Experiment [29]	Proposed Method	Error [%]
1	0.125	0.125	1.0003	0.9980	0.24	0.9991	0.9974	0.17	0.9967	0.9950	0.17
2	0.125	0.250	0.9994	0.9980	0.13	0.9944	0.9943	0.02	0.9840	0.9867	0.27
3	0.125	0.375	0.9969	0.9975	0.06	0.9847	0.9884	0.37	0.9582	0.9711	1.35
4	0.125	0.500	0.9946	0.9942	0.04	0.9648	0.9681	0.35	0.9199	0.9223	0.27
5	0.250	0.125	0.9972	0.9953	0.19	0.9926	0.9899	0.27	0.9940	0.9916	0.24
6	0.250	0.250	0.9887	0.9901	0.15	0.9725	0.9752	0.28	0.9786	0.9798	0.12
7	0.250	0.375	0.9717	0.9802	0.87	0.9311	0.9498	2.01	0.9507	0.9610	1.08
8	0.250	0.500	0.9432	0.9483	0.54	0.9904	0.8833	10.81	0.9080	0.9199	1.32
9	0.375	0.125	0.9943	0.9903	0.40	0.9986	0.9931	0.55	1.0003	1.0005	0.02
10	0.375	0.250	0.9737	0.9766	0.30	0.9811	0.9832	0.21	0.9991	0.9999	0.09
11	0.375	0.375	0.9356	0.9522	1.78	0.9566	0.9668	1.06	0.9976	0.9988	0.12
12	0.375	0.500	0.8485	0.8840	4.18	0.9219	0.9272	0.57	0.9955	0.9949	0.07
13	0.500	0.125	0.9883	0.9877	0.06	1.0005	1.0004	0.01	0.9925	0.9910	0.15
14	0.500	0.250	0.9601	0.9699	1.02	1.0005	1.0005	0.00	0.9725	0.9783	0.60
15	0.500	0.375	0.9172	0.9391	2.38	1.0002	1.0005	0.02	0.9456	0.9574	1.24
16	0.500	0.500	0.8269	0.8573	3.68	1.0002	0.9996	0.06	0.8927	0.9082	1.74

the experimental data reported by Silva and Gomes [29], for a total of 16 damage scenarios that include four different crack locations and four crack size levels at each location. Figures 9a–9c show the frequency response functions of the first three natural frequencies obtained using the proposed improved two-dimensional finite element plotted (in a three-dimensional plot) in the form of frequency ratio (ω_c/ω) versus the crack depth ratio (α/H) for various crack location ratios (c/L). Figures 10a–10c show the plots of the predicted variations of the first three natural frequencies as a function of the crack size, for some of the crack locations of the free-free beam. Similar to the observations reported by Li et al. [15], the present study shows that for all the cases considered, the natural frequencies decrease as the crack sizes increase. For some of the crack locations considered, the frequencies remained unchanged until a certain value of crack size ratio is attained, after which the frequencies decreases rapidly. For larger values of crack size ratio the frequency decreases rapidly.

Figures 11a–11c present the predicted variations of the first three natural frequencies as a function of the crack location. Since the frequency for a mode remains almost unchanged if the crack location coincides with the vibration node of that mode, when the crack is located at the center of the beam, the second natural frequency is almost unaffected. When the crack is located at $c/L = 1/3$ (or $c/L = 2/3$), the third natural frequency is almost unaffected. Similar observations were reported by Li et al. [15].
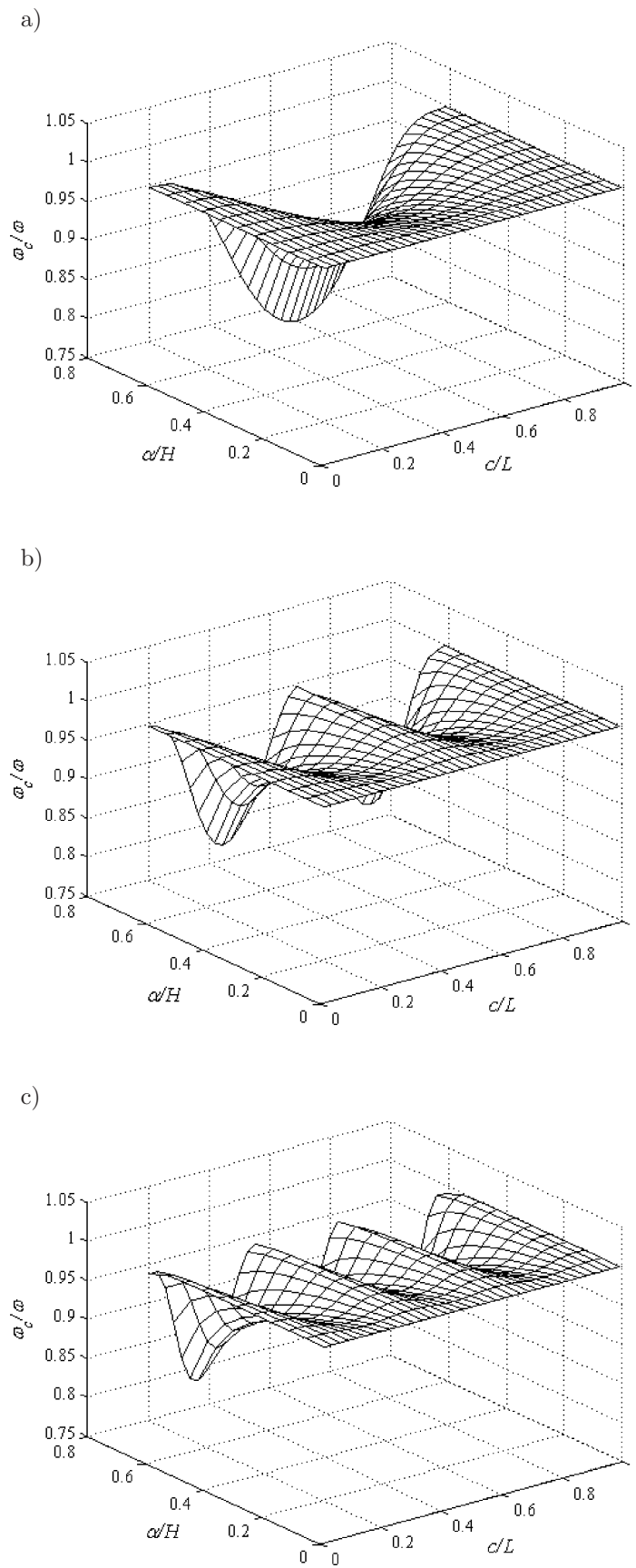
a)

b)

c)

Fig. 9. 3D plots of natural frequency ratio versus crack location, and size for free-free beam: a) Mode 1, b) Mode 2 and c) Mode 3.
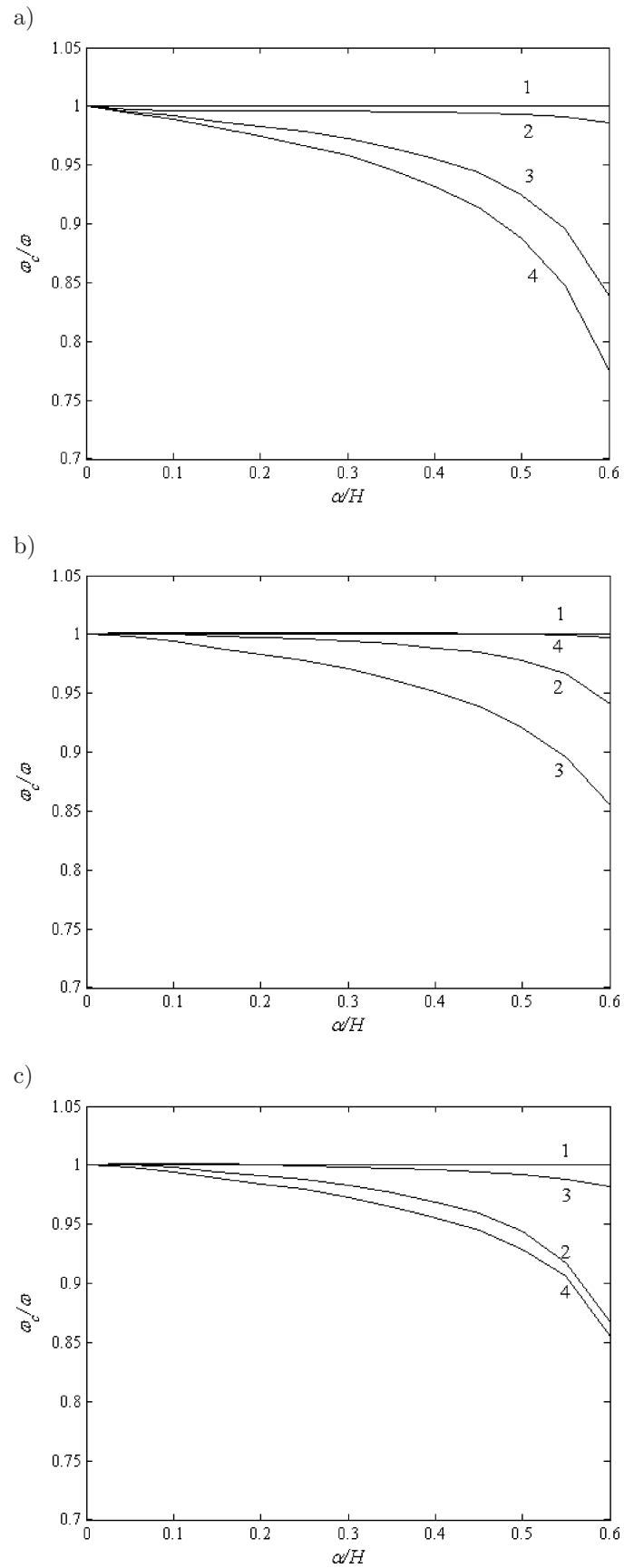
a)

b)

c)

Fig. 10. Natural frequency ratio versus crack size for free-free beam: a) Mode 1, b) Mode 2 and c) Mode 3 (1: uncracked, 2: $c/L = 1/8$, 3: $c/L = 1/3$ and 4: $c/L = 1/2$).
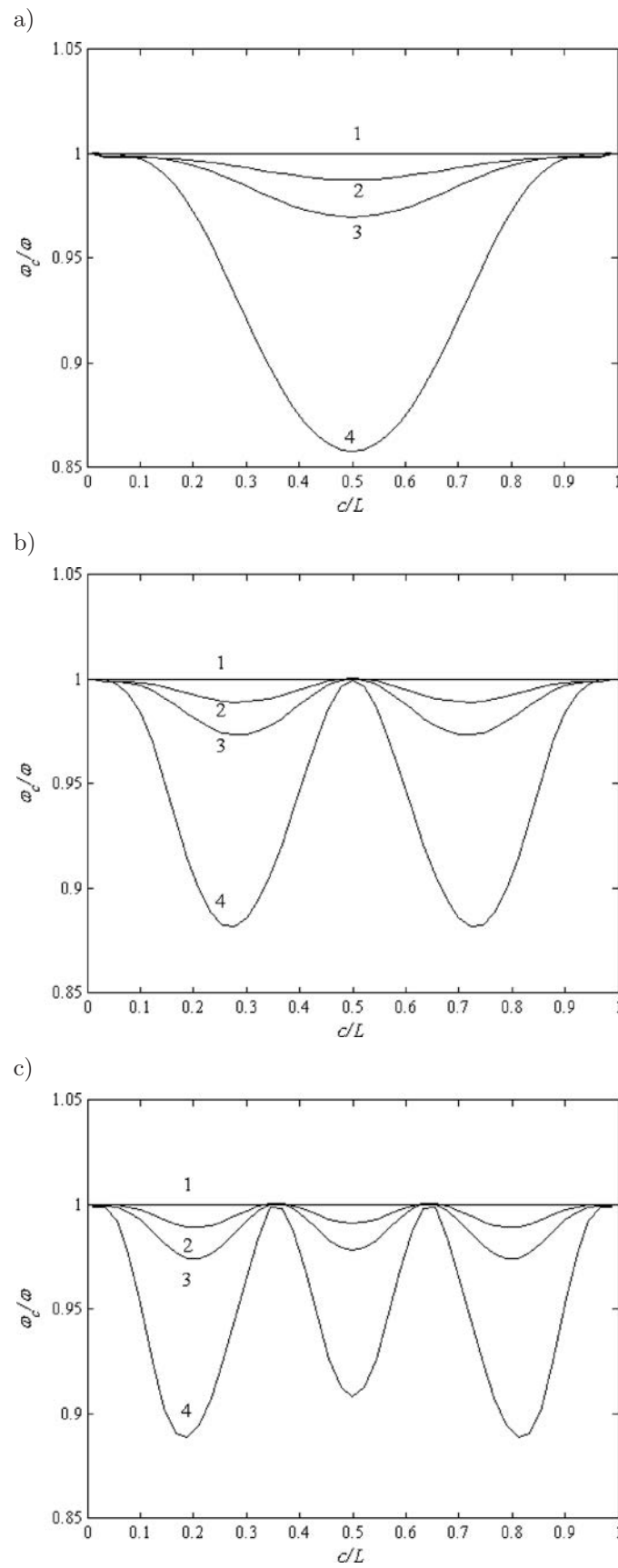
a)

b)

c)

Fig. 11. Natural frequency ratio versus crack location for free-free beam: a) Mode 1, b) Mode 2 and c) Mode 3 (1: uncracked, 2: $\alpha/H = 1/8$, 3: $\alpha/H = 1/4$ and 4: $\alpha/H = 1/2$).
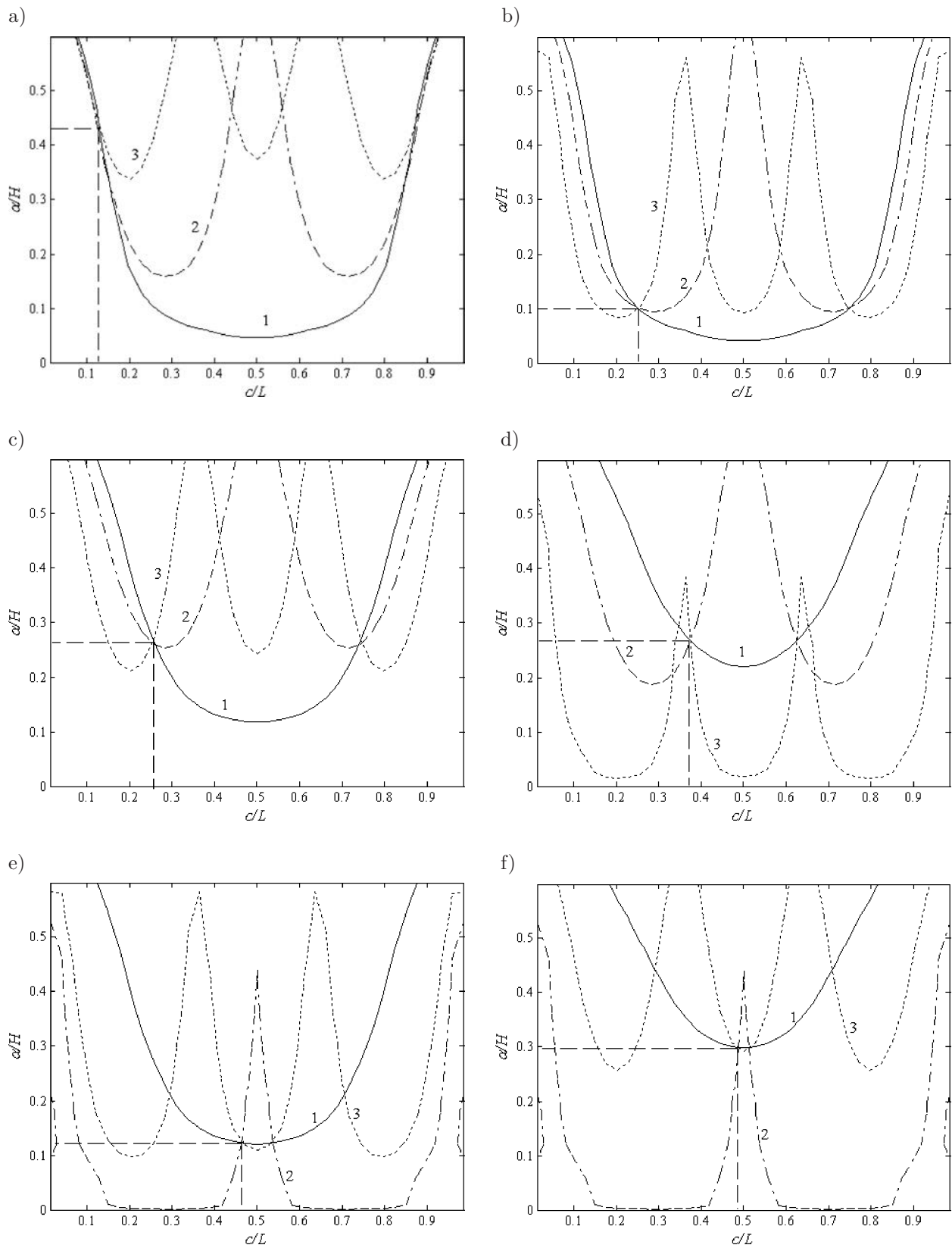
Fig. 12. Crack identification results for free-free beam: (a) case 3, (b) case 5, (c) case 6, (d) case 10, (e) case 13, and (f) case 14 (1: mode 1, 2: mode 2, 3: mode 3).

The method for crack identification is verified for several combinations of crack locations and crack sizes listed in Table 2. The first three natural frequencies measured by Silva and Gomes [29] are used as input in this case. Figures 12a–12f show the contour lines of the first three modes of free-free beam, for selected cases. The intersection of the three curves indicates the possible crack location and crack size. When the three curves do not meet exactly, the centroid [21] of the three pairs of intersections is taken as the crack location and crack size. Table 2 compares the predicted crack locations and crack sizes with the corresponding actual values. The predicted values are in good agreement with the corresponding actual values. It is worth noting that the average error in the crack location predictions is 1.20% and the average error in the crack size predictions is 5.72%, which is less when compared to the predictions reported by Li et al. [15].

Table 2. Comparison of predicted crack positions and sizes of free-free beam with corresponding actual values.

Crack case	Actual crack [29]		Predicted crack		Predicted error [%][a]	
	Location c/L	Size α/H	Location c/L	Size α/H	Location c/L	Size α/H
1	0.125	0.125	0.070	0.323	5.46	19.83
2	0.125	0.250	0.111	0.326	1.44	7.64
3	0.125	0.375	0.125	0.433	0.03	5.82
4	0.125	0.500	0.114	0.561	1.06	6.06
5	0.250	0.125	0.252	0.101	0.21	2.45
6	0.250	0.250	0.257	0.262	0.69	1.22
7	0.250	0.375	0.253	0.441	0.29	6.65
8	0.250	0.500	0.243	0.556	0.74	5.61
9	0.375	0.125	0.404	0.078	2.93	4.73
10	0.375	0.250	0.374	0.267	0.13	1.74
11	0.375	0.375	0.370	0.437	0.53	6.23
12	0.375	0.500	0.368	0.562	0.73	6.17
13	0.500	0.125	0.467	0.123	3.30	0.17
14	0.500	0.250	0.490	0.298	1.05	4.85
15	0.500	0.375	0.494	0.438	0.56	6.33
16	0.500	0.500	0.500	0.561	0.02	6.06

[a] Predicted error [%] = (Actual value – Predicted value) × 100.

5.2. Simply supported beam

Owolabi et al. [23] tested seven simply supported beam models with cracks at seven different locations, starting from a location nearer to one of the simply supported ends. The crack depth was varied from $0.1H$ to $0.7H$ (the depth of the beam, $H = 0.0254$ m) with an increment of $0.1H$ at each crack location. Each beam model was made of an aluminum bar of cross-sectional area 0.0254 m×0.0254 m with a length of 0.650 m. It had the following material properties: Young's modulus $E = 7 \times 10^{10}$ N/m^2, density $\rho = 2696$ kg/m^3, the Poisson ratio $\nu = 0.35$.

In the current study, the same beam is modeled with 101 standard four node elements ABAQUS [1] elements and one UEL at the top of the beam. Typical discretization of the simply supported beam is shown in Fig. 13. Figures 14a–14c show the frequency response functions of the first three natural frequencies obtained using the proposed improved two-dimensional finite element plotted (in a three-dimensional plot) in the form of frequency ratio (ω_c/ω) versus the crack depth ratio (α/H) for various crack location ratios (c/L). Figures 15a–15c show the plots of the predicted variations of the first three natural frequencies as a function of the crack size for some of the crack locations of simply supported beam.
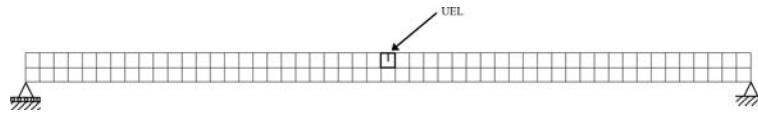
Fig. 13. Discretization of simply supported beam with surface crack using 101 standard four node ABAQUS elements and one UEL.
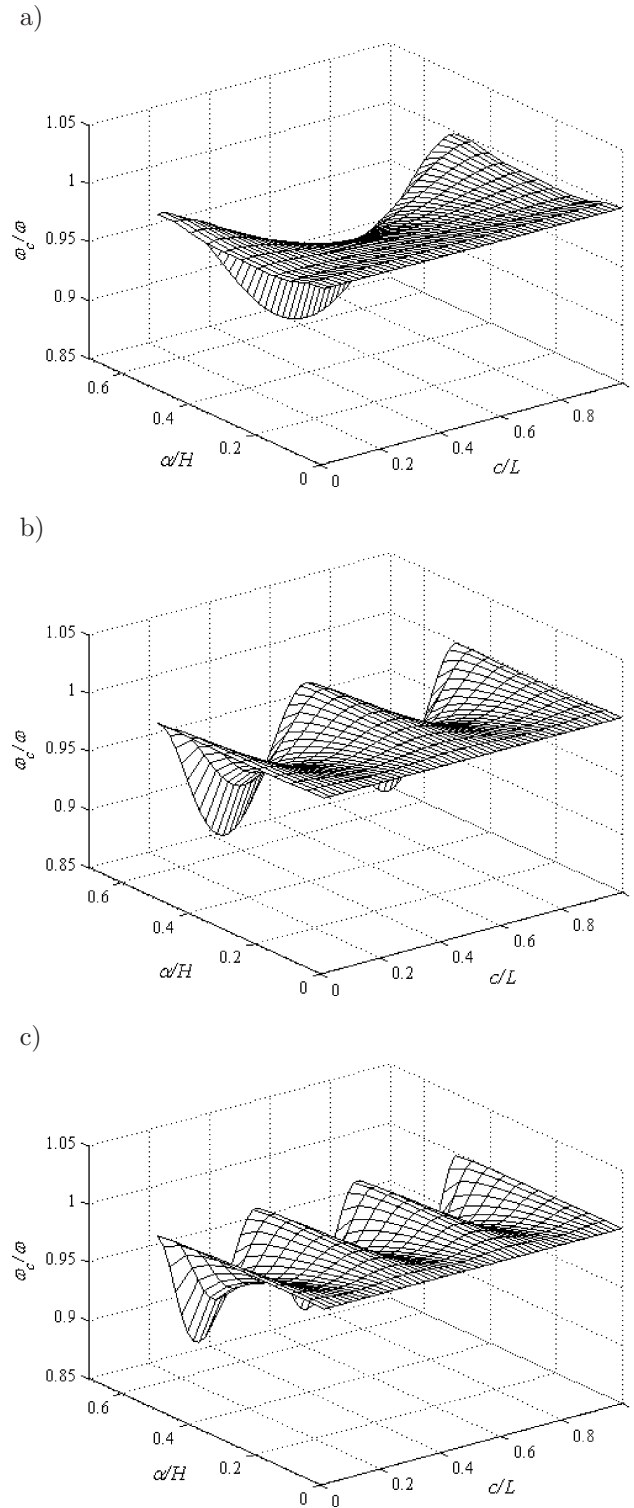
a)

b)

c)

Fig. 14. 3D plots of natural frequency ratio versus crack location, and size for simply supported beam: a) Mode 1, b) Mode 2, and c) Mode 3.
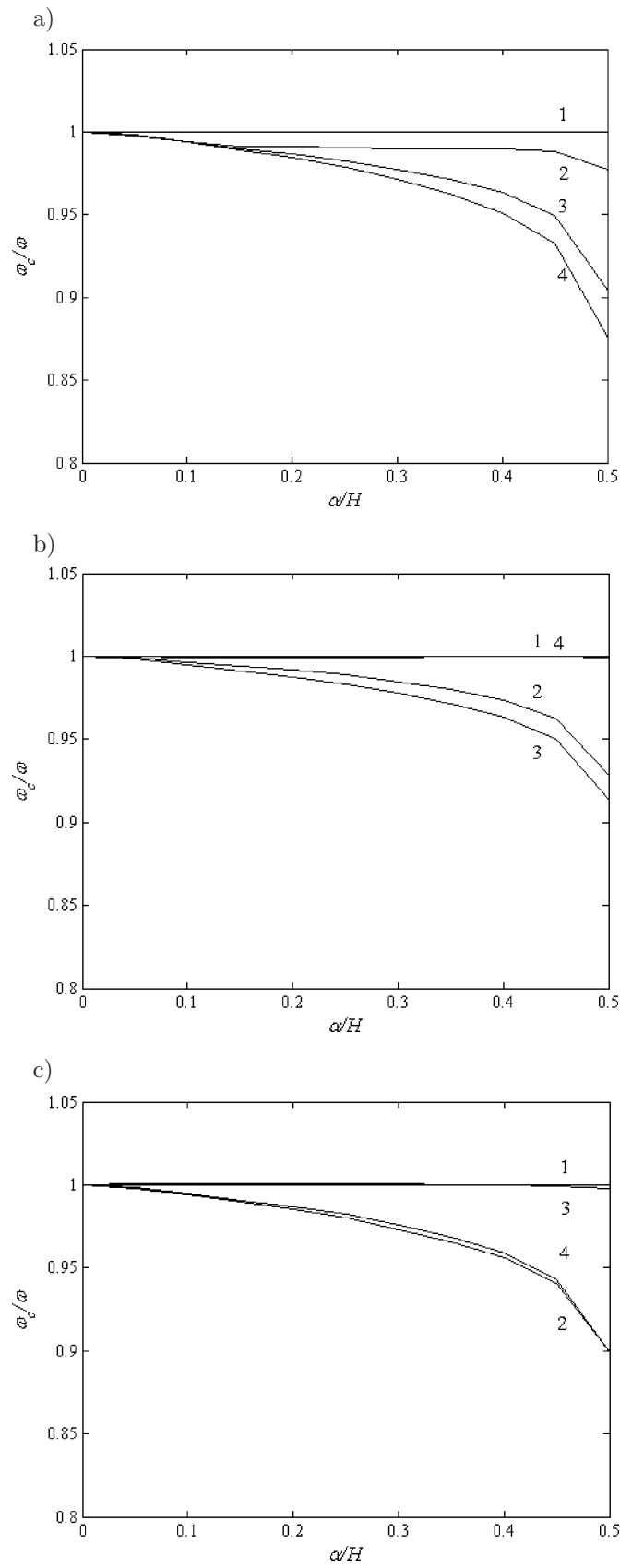
a)

b)

c)

Fig. 15. Natural frequency ratio versus crack size for simply supported beam: a) Mode 1, b) Mode 2 and c) Mode 3 (1: uncracked, 2: $c/L = 1/8$, 3: $c/L = 1/3$, and 4: $c/L = 1/2$).
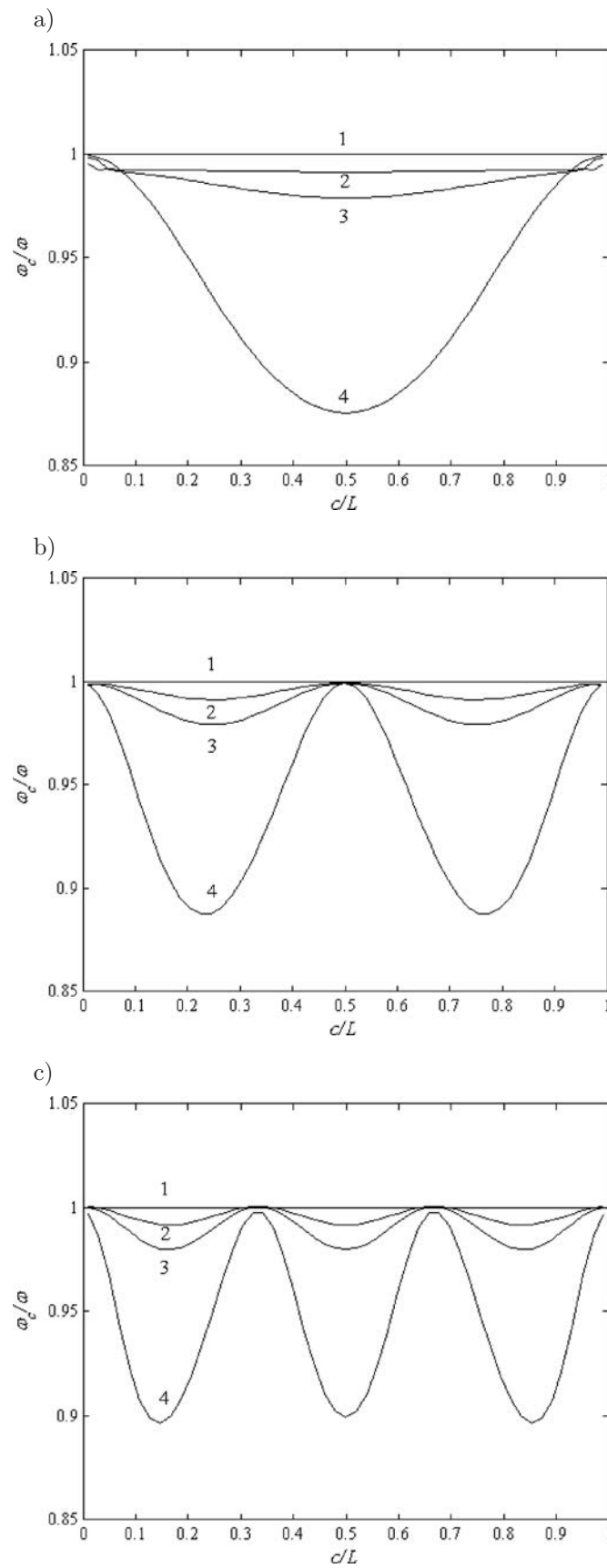
a)

b)

c)

Fig. 16. Natural frequency ratio versus crack location for simply supported beam: a) Mode 1, b) Mode 2, and c) Mode 3 (1: uncracked, 2: $\alpha/H = 1/8$, 3: $\alpha/H = 1/4$, and 4: $\alpha/H = 1/2$).

Figures 16a–16c present the predicted variations of the first three natural frequencies as a function of the crack location. Similar to the observations reported by Yang et al. [38], the present study shows that for the first mode, the maximum change of frequency takes place as the crack occurs at the midpoint of the beam. This is due to the fact that the dynamic bending moment is larger at the centre of the beam (where the amplitude of the first mode shape is greatest) and hence for the first mode, the presence of crack results in a greater loss of bending stiffness. However, the second and third modes are less affected at this location. The second and third mode frequencies change marginally for crack location ratios $c/L = 1/2$ and $c/L = 1/3$, respectively; this is due to the fact that these crack locations are respectively the vibration nodes of the second and third modes. The crack occurring near the ends of the beam does not change the frequencies.

Similar to that for free-free beam case, the method for crack identification is verified for several combinations of crack locations and crack sizes listed in Table 3. The first three natural frequencies measured by Owolabi et al. [23] are used as input in this case. Figures 17a–17f show the contour lines of the first three modes of simply supported beam for selected cases. The predicted crack locations and crack sizes are compared with the corresponding actual values in Table 3. The predicted crack locations and crack sizes are in good agreement with the actual values with the average error in the crack location and crack size predictions equal to 2.90% and 2.66%, respectively.

Table 3. Comparison of predicted crack positions and sizes of simply supported beam with corresponding actual values.

Crack case	Actual crack [23]		Predicted crack		Predicted error [%][a]	
	Location c/L	Size α/H	Location c/L	Size α/H	Location c/L	Size α/H
1	0.1875	0.10	0.283	0.053	9.52	4.74
2	0.1875	0.20	0.251	0.137	6.36	6.32
3	0.1875	0.30	0.247	0.239	5.91	6.05
4	0.1875	0.40	0.202	0.387	1.40	1.32
5	0.1875	0.50	0.247	0.463	5.91	3.68
6	0.3125	0.10	0.204	0.076	10.87	2.37
7	0.3125	0.20	0.289	0.134	2.30	6.58
8	0.3125	0.30	0.310	0.287	0.27	1.32
9	0.3125	0.40	0.321	0.416	0.86	1.58
10	0.3125	0.50	0.326	0.476	1.31	2.37
11	0.4375	0.10	0.434	0.074	0.37	2.63
12	0.4375	0.20	0.452	0.229	1.44	2.90
13	0.4375	0.30	0.445	0.332	0.76	3.16
14	0.4375	0.40	0.438	0.408	0.09	0.79
15	0.4375	0.50	0.438	0.482	0.09	1.84
16	0.5000	0.10	0.477	0.082	2.33	1.84
17	0.5000	0.20	0.497	0.184	0.30	1.58
18	0.5000	0.30	0.470	0.339	3.01	3.95
19	0.5000	0.40	0.497	0.421	0.30	2.11
20	0.5000	0.50	0.481	0.484	1.88	1.58

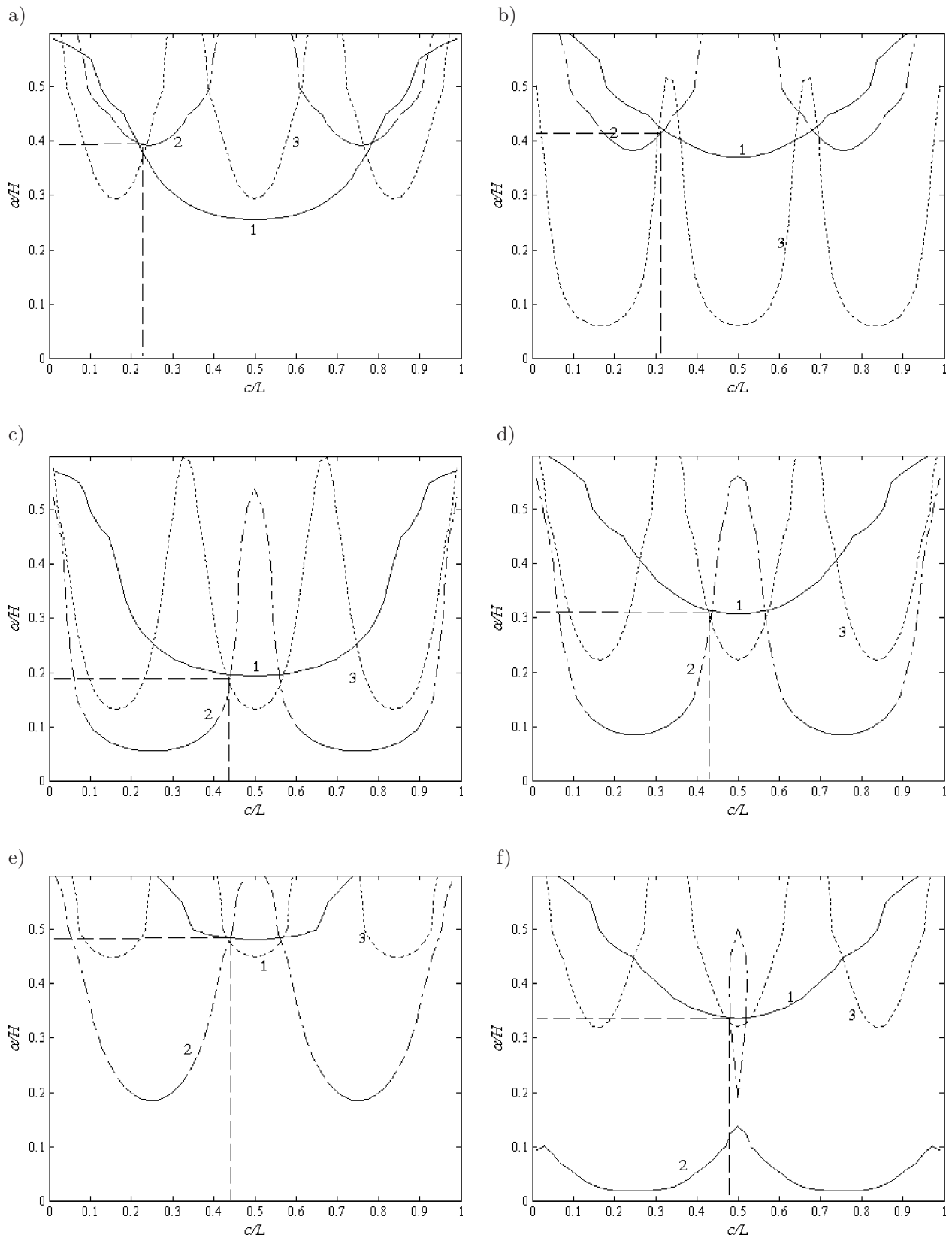[a] Predicted error [%] = (Actual value – Predicted value) × 100.

Fig. 17. Crack identification results for simply supported beam: a) case 4, b) case 9, c) case 12, d) case 13, e) case 15, and f) case 18 (1: mode 1, 2: mode 2, 3: mode 3).

5.3. Fixed-fixed beam

Similar to the simply supported beam models, Owolabi et al. [23] also tested seven fixed-fixed beam models having the same geometrical and material properties with cracks at seven different locations, starting from a location nearer to one of the clamped end. In the current study the fixed-fixed beam is modeled with the same discretization as shown in Fig. 13. Figures 18a–18c show the
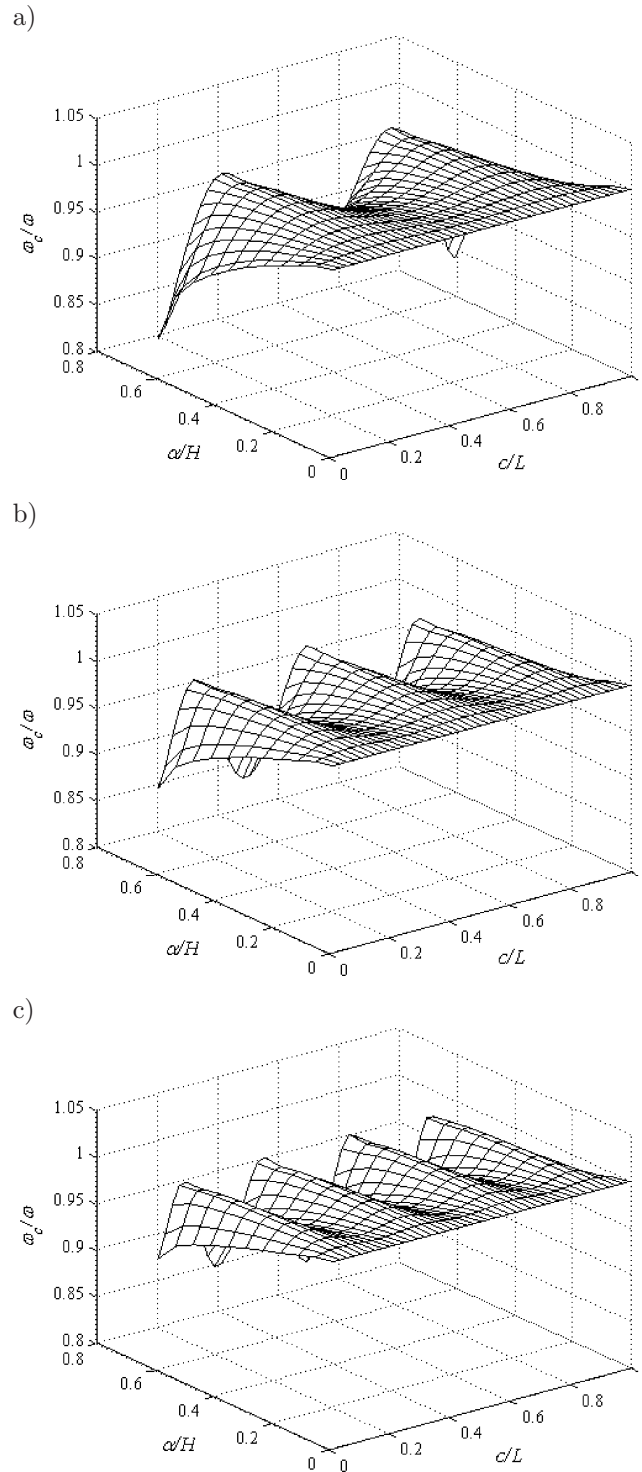
a)

b)

c)

Fig. 18. 3D plots of natural frequency ratio versus crack location, and size for fixed–fixed beam: (a) Mode 1, (b) Mode 2 and (c) Mode 3.

frequency response functions of the first three natural frequencies. Figures 19a–19c show the plots of the predicted variations of the first three natural frequencies as a function of the crack size for some of the crack locations of fixed-fixed beam.
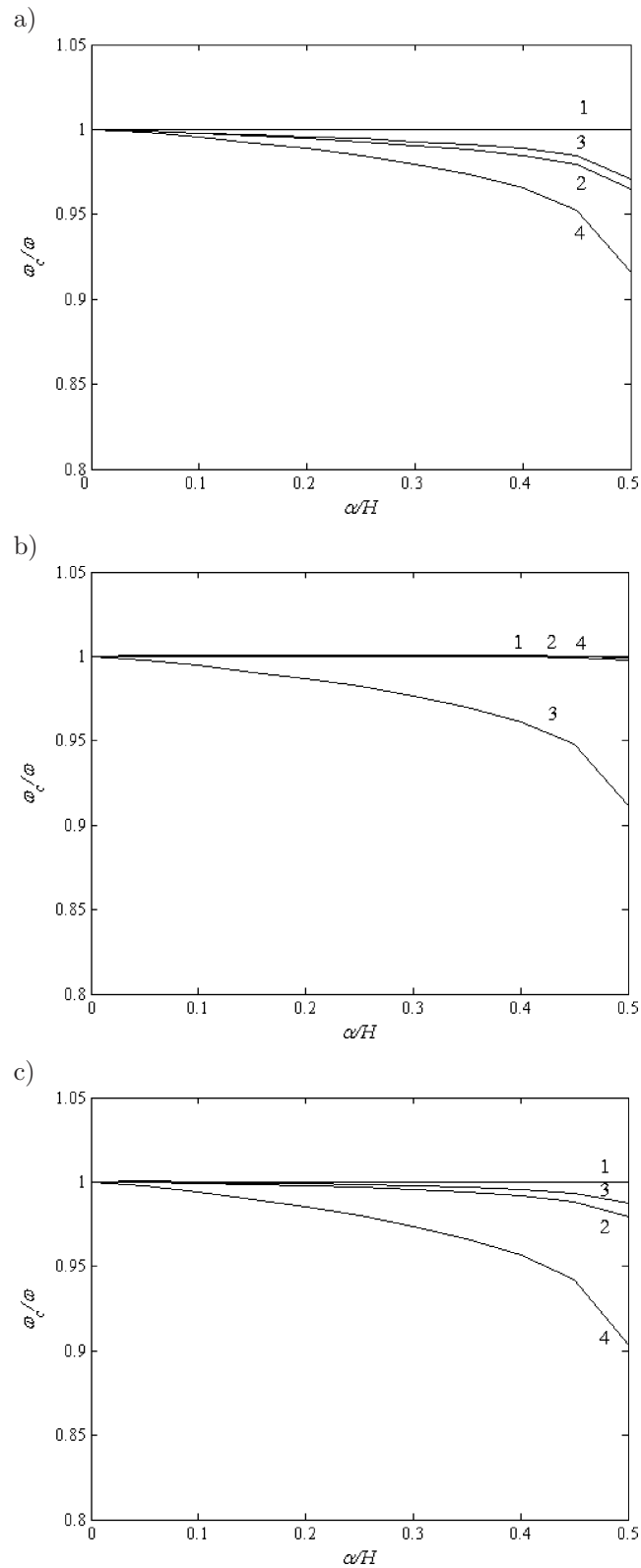
a)

b)

c)

Fig. 19. Natural frequency ratio versus crack size for fixed-fixed beam: a) Mode 1, b) Mode 2 and c) Mode 3 (1: uncracked, 2: $c/L = 1/8$, 3: $c/L = 1/3$, and 4: $c/L = 1/2$).

Figures 20a–20c present the predicted variations of the first three natural frequencies as a function of the crack location. Unlike the simply supported beam, the maximum changes of frequencies
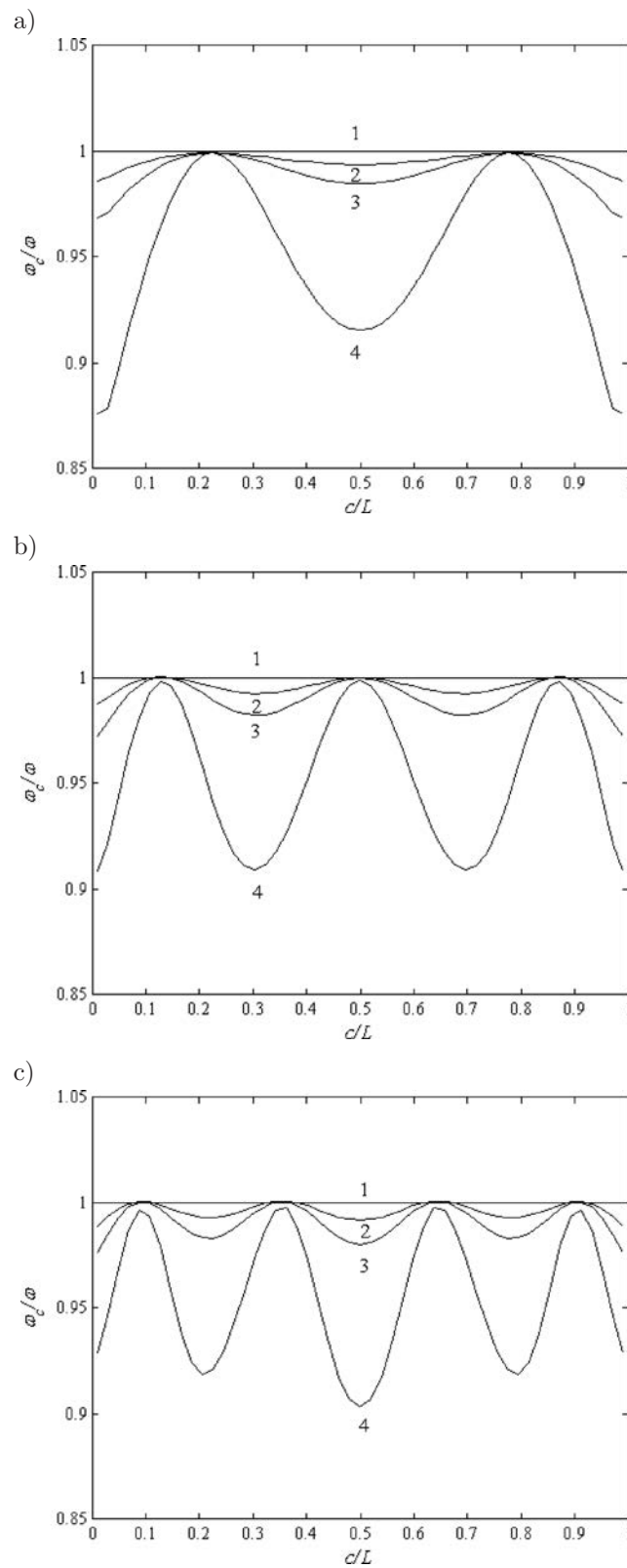

Fig. 20. Natural frequency ratio versus crack location for fixed-fixed beam: a) Mode 1, b) Mode 2 and c) Mode 3 (1: uncracked, 2: $\alpha/H = 1/8$, 3: $\alpha/H = 1/4$, and 4: $\alpha/H = 1/2$).

occur when the crack is near the ends of the beam. The reason is that the maximum bending moment occurs near the support in the case of a fixed-fixed beam, and the presence of a crack at these locations would reduce the stiffness near the supports (the boundary constraints). Similar observations were reported by Yang et al. [38]. The first and third mode frequencies also show higher decrease for the crack located at the centre of beam due to higher bending moment at these locations. However for the second mode, the change in frequency is negligible because the centre of beam is the node of the second mode of vibration. In addition, for fixed-fixed beam frequency changes are also observed to be very low at those points where the dynamic bending moments are least. Thus, the change in frequency is not only a function of the crack location and size, but also of mode number, distance to mode shape node, etc.

Similar to that for simply supported beam case, using the first three natural frequencies measured by Owolabi et al. [23] are used as input, the method for crack identification is verified for several combinations of crack locations and crack sizes listed in Table 4. Figures 21a–21f show the contour lines of the first three modes of simply supported beam for selected cases. Comparison of the predicted crack locations and crack sizes with the corresponding actual values in Table 4 shows that the predicted values are in good agreement with the actual values. The average error in the crack location predictions is 2.76% and the average error in the crack size predictions is 2.93%.

Table 4. Comparison of predicted crack positions and sizes of simply supported beam with corresponding actual values.

Crack case	Actual crack [23]		Predicted crack		Predicted error [%][a]	
	Location c/L	Size α/H	Location c/L	Size α/H	Location c/L	Size α/H
1	0.1875	0.10	0.252	0.059	6.45	4.08
2	0.1875	0.20	0.284	0.143	9.62	5.75
3	0.1875	0.30	0.195	0.283	0.80	1.71
4	0.1875	0.40	0.227	0.406	3.97	0.57
5	0.1875	0.50	0.225	0.461	3.74	3.95
6	0.3125	0.10	0.388	0.090	7.53	1.01
7	0.3125	0.20	0.280	0.145	3.29	5.53
8	0.3125	0.30	0.300	0.298	1.30	0.17
9	0.3125	0.40	0.311	0.425	0.16	2.54
10	0.3125	0.50	0.311	0.476	0.16	2.41
11	0.4375	0.10	0.417	0.064	2.03	3.64
12	0.4375	0.20	0.438	0.191	0.01	0.92
13	0.4375	0.30	0.433	0.318	0.45	1.80
14	0.4375	0.40	0.426	0.423	1.13	2.33
15	0.4375	0.50	0.438	0.485	0.01	1.54
16	0.5000	0.10	0.427	0.092	7.29	0.79
17	0.5000	0.20	0.492	0.114	0.75	8.60
18	0.5000	0.30	0.478	0.320	2.17	2.02
19	0.5000	0.40	0.468	0.432	3.23	3.20
20	0.5000	0.50	0.460	0.493	3.98	0.66

[a] Predicted error [%] = (Actual value – Predicted value) × 100.
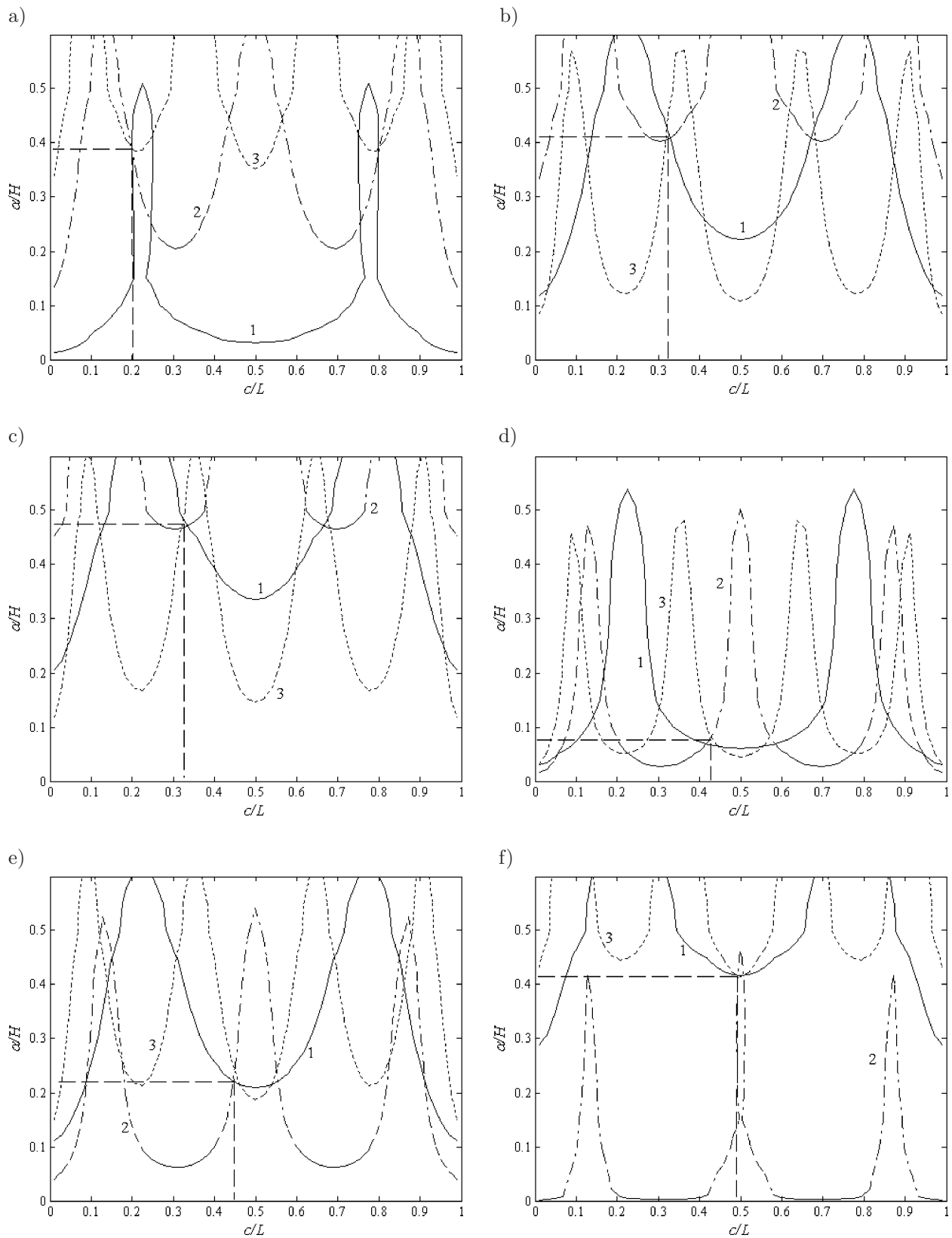
a)

b)

c)

d)

e)

f)

Fig. 21. Crack identification results for fixed-fixed beam: a) case 4, b) case 9, c) case 10, d) case 11, e) case 12, and f) case 19 (1: mode 1, 2: mode 2, 3: mode 3).

6. Conclusions

This paper presents an improved two-dimensional finite element with an embedded edge crack for crack depth ratios ranging up to 0.9 and for predicting natural frequency of a cracked beam more accurately. The FRANC2DL finite element code is used with the J-integral option to extract the stress intensity factors from stress strain fields around the crack tip location. The geometric factors for various loading cases of the cracked element for crack depth ratios ranging up to 0.9 are obtained by means of curve fitting techniques, and they are subsequently used to obtain the components of the stiffness matrix for the cracked element from the Castigliano's first theorem using fracture mechanics concepts. The element is implemented in the commercial finite element code ABAQUS as user element subroutine. The first natural frequency for the bending mode for several beam cases with different damage locations, obtained using the proposed improved finite element are in good agreement with the available experimental data. A methodology to detect crack location and size in conjunction with the proposed improved cracked element is also presented for singularity problems like a cracked beam. The frequency response functions are approximated by means of surface fitting techniques as a function of the crack location and size. Measured natural frequencies are used in a crack detection process and the crack location and size can be identified by finding the point of intersection of three frequency contour lines. In addition, the experimental data from beams studied by other researchers is employed to verify the accuracy of the proposed methodology in the diagnosis of structural crack faults. The predicted crack locations and crack sizes are in good agreement with the actual values.

Acknowledgement

References

[1] ABAQUS version 6.5. Hibbit, Karlson & Sorensen, Inc., Pawtucket, RI (USA), 2004.

[2] S. Chinchalkar. Determination of crack location in beams using natural frequencies. *J. Sound Vib.*, **247**(3): 417–429, 2001.

[3] T.G. Chondros, A.D. Dimarogonas, J. Yao. A continuous cracked beam vibration theory. *J. Sound Vib.*, **215**: 17–34, 1998.

[4] T.G. Chondros, A.D. Dimarogonas, J. Yao. Vibration of a beam with a breathing crack. *J. Sound Vib.*, **239**: 57–67, 2001.

[5] M. Dilena, A. Morassi. The use of antiresonances for crack detection in beams. *J. Sound Vib.*, **276**: 195–214, 2004.

[6] M. Dilena, A. Morassi. Damage detection in discrete vibrating systems. *J. Sound Vib.*, **289**: 830–850, 2006.

[7] M. Dilena, A. Morassi. Identification of crack location in vibrating beams from changes in node positions. *J. Sound Vib.*, **255**(5): 915–930, 2002.

[8] S.W. Doebling, C.R. Farrar, M.B. Prime, D.W. Shevitz. Damage Identification and Health Monitoring of Structural and Mechanical Systems from Changes in Their Vibration Characteristics: A Literature Review. Los Alamos National Laboratory, Los Alamos, NM, Technical Report LA-13070-MS, 1996.

[9] G. Dong, J. Chen, J. Zou. Parameter identification of a rotor with an open crack. *Eur. J. Mech. A Solids*, **23**: 325–333, 2004.

[10] S. Gondhalekar. Development of a software tool for crack propagation analysis in two dimensional layered structures. M.S. Thesis, Kansas State University, 1992.

[11] G.D. Gounaris, C.A. Papadopoulos, A.D. Dimarogonas. Crack identification in beams by coupled response measurements. *Comp. Struct.*, **58**: 299–305, 1996.

[12] M.A. James, D.V. Swenson. A software framework for two dimensional mixed mode- I/II elastic-plastic fracture. *Mixed-Mode Crack Behavior*, ASTM STP 1359, K. J. Miller and D. L. McDowell, Eds., Am. Soc. Test. Mats, West Conshohocken, PA, 111–126, 1999.

[13] M. Krawczuk, M. Palacz, W. Ostachowicz. The dynamic analysis of a cracked Timoshenko beam by the spectral element method. *J. Sound Vib.*, **264**: 1139–1153, 2003.

[14] S.P. Lele, S.K. Maiti. Modelling of transverse vibration of short beams for crack detection and measurement of crack extension. *J. Sound Vib.*, **257**(3): 559–583, 2002.

[15] B. Li, X. Chen, J. Ma, Z. He. Detection of crack location and size in structures using wavelet finite element methods. *J. Sound Vib.*, **285**: 767–782, 2005.

[16] R.Y. Liang, F.K. Choy, J. Hu. Detection of cracks in beam structures using measurements of natural frequencies. *J. Franklin Inst.*, **328**(4): 505–518, 1991.

[17] M.A. Mahmoud, M. Abu Zaid, S. Al Harashani. Numerical frequency analysis of uniform beams with a transverse crack. *Comm. Num. Meth. Eng.*, **15**: 709–715, 1999.

[18] MATLAB version 7.10. The Mathworks Inc., Natwick, MA (USA), 2010.

[19] D. Montalvao, N.M.M. Maia, A.M.R. Ribeiro. A review of vibration-based structural health monitoring with special emphasis on composite materials. *Shock Vib. Digest*, **38**(4): 295–324, 2006.

[20] A. Morassi. Identification of a crack in a rod based on changes in a pair of natural frequencies. *J. Sound Vib.*, **242**(4): 577–596, 2001.

[21] B.P. Nandwana, S.K. Maiti. Modelling of vibration of beam in presence of inclined edge or internal crack for its possible detection based on frequency measurements. *Engg. Frac. Mech.*, **58**(3): 193–205, 1997.

[22] P.G. Nikolakopoulos, D.E. Katsareas, C.A. Papadopoulos. Crack identification in frame structures. *Comp. Struct.*, **64**(1–4): 389–406, 1997.

[23] G. Owolabi, A. Swamidas, R. Seshadri. Crack detection in beams using changes in frequencies and amplitudes of frequency response functions. *J. Sound Vib.*, **265**: 1–22, 2003.

[24] C.A. Papadopoulos, A.D. Dimarogonas. Coupled longitudinal and bending vibrations of a rotating shaft with an open crack. *J. Sound Vib.*, **117**: 81–93, 1987.

[25] D.P. Patil, S.K. Maiti. Detection of multiple cracks using frequency measurements. *Engg. Frac. Mech.*, **70**(12): 1553–1572, 2003.

[26] G.P. Potirniche, J. Hearndon, S.R. Daniewicz, D. Parker, P. Cuevas, P.T. Wang, M.F. Horstemeyer. A two-dimensional damaged finite element for fracture applications. *Engg. Frac. Mech.*, **75**: 3895–3908, 2008.

[27] O.S. Salawu. Detection of structural damage through changes in frequency: A review. *Engg. Struct.*, **19**(9): 718–723, 1997.

[28] E.I. Shifrin, R. Ruotolo. Natural frequencies of a beam with an arbitrary number of cracks. *J. Sound Vib.*, **222**(3): 409–423, 1999.

[29] J.M. Silva, A.J.L. Gomes. Experimental dynamic analysis of cracked free-free beams. *Exp. Mech.*, **30**(1): 20–25, 1990.

[30] J.-J. Sinou. Damage assessment based on the frequencies' ratio surfaces intersection method for the identification of the crack depth, location and orientation. *Struct. Dur. Health Monitor*, **3**(3:) 134–162, 2007-a.

[31] J.-J. Sinou. Numerical investigations of a robust identification of crack location and size in beams using only changes in ratio pulsations of the cracked beams. *Struct. Eng. Mech.*, **25**(6): 691–716, 2007-b.

[32] H. Sohn, C. Farrar, F. Hemez, D. Shunk, D. Stinemates, B. Nadler. A review of structural health monitoring literature: 1996–2001. Los Alamos National Laboratory, Los Alamos, NM, Technical Report LA-13976-MS, 2003.

[33] A. Swamidas, X. Yang, R. Seshadri. Identification of cracking in beam structures using Timoshenko and Euler formulations. *J. Eng. Mech., ASCE*, **130**(11): 1297–1308, 2004.

[34] H. Tada, P.C. Paris, G.R. Irwin. The Stress Analysis of Cracks Handbook, 3 edition, ASME Press, Am. Soc. Mech. Eng. Three Park Avenue, New York, NY, 2000.

[35] P.A. Wawrzynek, A.R. Ingraffea. Interactive finite element analysis of fracture processes: an integrated approach. *Theor. Appl. Fract. Mech.*, **8**: 137–150, 1987.

[36] P.A.Wawrzynek, A.R. Ingraffea. FRANC2D: Two-dimensional crack propagation simulator, Version 2.7 User's Guide. NASA CR 4572, 1994.

[37] D. Wendtland. Änderung der biegeegenfrequenzen einer idealisierten Schaufel durch Risse. Ph.D. Dissertation, University of Karlsruhe, 1972.

[38] X.F. Yang, A.S.J. Swamidas, R. Seshadri. Crack identification in vibrating beams using the energy method. *J. Sound Vib.*, **244**(2): 339–357, 2001.